Journal of Membrane Science 541 (2017) 519–528

Contents lists available at ScienceDirect

Journal of Membrane Science

journal homepage: www.elsevier.com/locate/memsci

Optimization of dialyzer design to maximize solute removal with a two-dimensional transport model

Danilo Donato[a,b], Adriana Boschetti-de-Fierro[b], Carina Zweigart[b], Michael Kolb[b], Sunny Eloot[c], Markus Storr[b], Bernd Krause[b], Ken Leypoldt[d], Patrick Segers[a,*]

[a] IBiTech – bioMMeda, Department of Electronics and Information Systems, iMinds Medical IT, Ghent University, Campus Heymans (UZ), Blok B, De Pintelaan 185, B-9000 Ghent, Belgium

[b] Research and Development, Gambro Dialysatoren GmbH (Gambro Dialysatoren GmbH is part of Baxter International Inc), Holger-Crafoord-Str. 26, 72379 Hechingen, Germany

[c] Nephrology, Dialysis unit 1P8, Ghent University Hospital, De Pintelaan 185, B-9000 Ghent, Belgium

[d] Renal Therapeutic Area, Baxter Healthcare Corporation, DF5-1E, One Baxter Parkway, Deerfield, IL 60015, USA

ARTICLE INFO

Keywords:
Dialyzer
Model
Design optimization
Transport
Solute removal

ABSTRACT

A systematic analysis of the effect of all the dialyzer-related factors on solute clearance has not been reported in the literature, making it difficult to optimize dialyzer design to maximize solute removal from patient's blood. In this paper, a two-dimensional axisymmetric mathematical model of momentum and mass transport in dialyzers is proposed to investigate the effect of the most relevant geometrical and operational dimensionless groups on solute clearance. Navier-Stokes and Darcy-Brinkman equations are used to describe steady-state momentum transport in blood and dialysate compartments, and across the membrane, respectively. Transport of low and middle molecular weight solutes from the blood through the membrane into the dialysate compartment is described with convection-diffusion equations. The effect of non-Newtonian blood behavior and concentration polarization is also taken into account. The complete set of dimensionless groups determining dialyzer efficiency is obtained from dimensional analysis of model equations. Their effect on solute clearances is investigated by solving model equations for values of geometrical and operational dimensionless groups typical in clinical practice. The most relevant dimensionless groups determining dialyzer efficiency were identified and a novel design approach to optimize dialyzers in order to maximize solute clearances in a cost-effective way is proposed based on their values.

1. Introduction

Despite its existence for many decades, treatment of chronic renal failure with hemodialysis could still benefit from the development of optimized membrane modules for the effective removal of low and middle molecular weight toxins from the blood. During hemodialysis, low molecular weight water soluble solutes (such as urea) are mostly removed by diffusion, whereas the removal of middle molecular weight solutes (such as β_2-microglobulin and myoglobin) generally requires the superimposition of convective transport over pure diffusion by means of ultrafiltration (i.e. net weight loss of the patient) and hemofiltration (i.e. filtration of the substitution flow during pre and post-dilution hemodiafiltration). As a result, the efficiency of hollow fiber dialyzers depends on their ability to combine diffusive and convective transport to maximize solute clearance [1]. Solute transport in dialyzers is particularly affected by dialyzer geometry, membrane properties and operating conditions [2]. Optimization of membrane modules with in vitro experiments is limited by the difficult prediction of the extent to which membrane transport properties and module fluid dynamics influence solute clearance [3]. This is mostly due to the difficulty in mimicking of the transport phenomena occurring in vivo with aqueous systems and to the high economic costs needed to generate several modules to optimize dialyzer geometry.

Mathematical models of solute transport in dialyzers may help investigate how module design and operating conditions affect dialyzer efficiency and develop optimized membranes and modules while reducing R & D and manufacturing costs. In the last 30 years, several mathematical models have been proposed to describe transport phenomena in dialyzers.

* Corresponding author.
E-mail addresses: danilo_donato@baxter.com (D. Donato), adriana_boschetti@baxter.com (A. Boschetti-de-Fierro), carina_zweigart@baxter.com (C. Zweigart), michael_kolb@baxter.com (M. Kolb), sunny.eloot@ugent.be (S. Eloot), markus_storr@baxter.com (M. Storr), bernd_krause@baxter.com (B. Krause), kenleypoldt@gmail.com (K. Leypoldt), patrick.segers@ugent.be (P. Segers).

http://dx.doi.org/10.1016/j.memsci.2017.07.018
Received 25 April 2017; Received in revised form 3 July 2017; Accepted 9 July 2017
Available online 11 July 2017
0376-7388/

Nomenclature

$A_{tot} = \pi d_B LN$ total membrane surface area [m^2]
$C_{i,j}$ molar concentration of the j-th solute in the i-th compartment [mol/m^3]
Cl_j clearance of the j-th solute [m^3/s]
C_p protein concentration [g/l]
d_B fiber inner diameter [m]
d_H housing diameter [m]
$D_{i,j}$ j-th solute diffusivity in the i-th compartment [m^2/s]
H_{in} inlet hematocrit [-]
$k_{c,p}$ protein mass transfer coefficient [m/s]
k_m membrane Darcy permeability [m^2]
K_{UF} ultrafiltration coefficient [m^3/(s*Pa)]
L effective module length [m]
L_p membrane hydraulic permeability [m^2s/kg]
MW_j molecular weight of the j-th solute [kg/mol]
N number of fibers [–]
P_i pressure in the i-th compartment [Pa]
PD module packing density [–]
$Pe_{ax,max,j}$ maximal axial Peclet number [–]
$Pe_{r,max,j}$ maximal reduced Peclet number [–]
Q_B total blood flow rate in blood compartment [m^3/s]
Q_D total dialysate flow rate in blood compartment [m^3/s]
Q_{UF} total net ultrafiltration rate [m^3/s]
r radial coordinate [m]
Re_B Reynolds number in the blood compartment [–]
S_j sieving coefficient of the j-th solute [–]
Sc Schmidt number [–]
Sh Sherwood number [–]
T temperature [K]
u_i axial velocity in the i-th compartment [m/s]
$u_{in,B} = 4Q_B/(N\pi d_B^2)$ average axial velocity at blood-side entrance [m/s]
v_i radial velocity in the i-th compartment [m/s]
z axial coordinate [m]

Superscripts and subscripts

* dimensionless
B blood
b membrane bulk
β2m β2-microglobulin
creat creatinine
D dialysate
eff effective
i i-th compartment (B, m_s, m_b, D)
in inlet
j j-th solute
λ λ-th membrane layer (λ = b, s)
m membrane
myo myoglobin
p protein
pl plasma
out outlet
RBC red blood cells
s membrane skin
urea urea
w wall

Greek symbols

α pressure modulus [–]
δ_D thickness of the dialysate compartment [m]
$\delta_m = \delta_{m,b} + \delta_{m,s}$ total membrane thickness [m]
$\varepsilon_{m,i}$ membrane i-th layer porosity [–]
μ_i fluid viscosity in the i-th compartment [Pa s]
$\mu_{B,in} = \mu_{pl}(1 + 2.5H_{in})$ reference viscosity in blood compartment [Pa s]
π oncotic pressure [Pa]
π_0 oncotic pressure at Cp = Cp_{in} [Pa]
$\rho_{B,in} = \rho_{pl}(1\text{-}H_{in}) + \rho_{RBC}H_{in}$ reference density in blood compartment [kg/m^3]
ρ_i fluid density in the i-th compartment [kg/m^3]

Some models provide a simplified description of transport phenomena based on a uniform profile of ultrafiltration flux allowing for the analytical solution of model equations [4–6], or describing solute transport from the blood bulk to the membrane outer surface, across the porous membrane and from the membrane outer surface towards the dialysate bulk in terms of an overall mass transfer coefficient [3,4,6–10]. The accumulation of partially rejected solutes at the membrane wall has been generally neglected [4,6,11,13], as well as the non-Newtonian blood behavior [3,4,6,12]. Only few of these models have been used to determine the influence of certain dialyzer parameters on solute clearance, such as overall mass transfer coefficient [6], blood and dialysate flow rates [3,14], ultrafiltration flow rate [3,10], hydraulic and diffusive permeability [10], fiber inner diameter and active module length [10,13], inlet and outlet geometrical structures [14,15].

To the best of the authors' knowledge, a systematic and in-depth analysis of the influence of the dialyzer-related factors accounting for module geometry, membrane transport properties and operating conditions on solute transport has yet to be reported. This hinders to identify the interplay among the most relevant parameters determining dialyzer efficiency and makes it difficult to optimize dialyzer design for maximal solute removal.

In this paper, a two-dimensional mathematical transport model is presented aimed to (i) identify the most relevant dialyzer-related factors determining dialyzer efficiency and (ii) investigate how their interplay influences solute clearance in order to optimize dialyzer design. Navier-Stokes and Darcy-Brinkman equations were used to describe momentum transport in all the compartments of the dialyzer (i.e. blood-side, dialysate -side, membrane), respectively, whereas the convection-diffusion equation was used to describe the transport of low and middle molecular weight solutes in each dialyzer compartment. Non-Newtonian blood behavior and effect of concentration polarization were also taken into account. Dimensional analysis was used to identify the dimensionless groups determining dialyzer efficiency and their effect on solute clearance was investigated by solving model equations under working conditions typical in clinical practice. A reference framework based on model predictions is proposed to help develop dialyzers allowing for the maximization of solute clearances in a cost-effective way.

2. Methods

2.1. Model development

A scheme of a hollow fiber dialyzer is shown in Fig. 1. A bundle of around 10,000 hollow fibers is contained in an external housing. Blood flows into the lumen of the hollow fibers while dialysate, an aqueous electrolyte solution, flows countercurrent around the fibers. Solute transport across the fiber semi-permeable membrane and between the blood and dialysate occurs both by diffusion and convection. In the model presented in this paper, it is assumed that the fibers are evenly spaced and arranged in regular hexagonal arrays, and each fiber is surrounded by a uniform annulus. The interstitial spaces among neighboring annuli are neglected. It is important to remark that non-uniform fiber spacing would

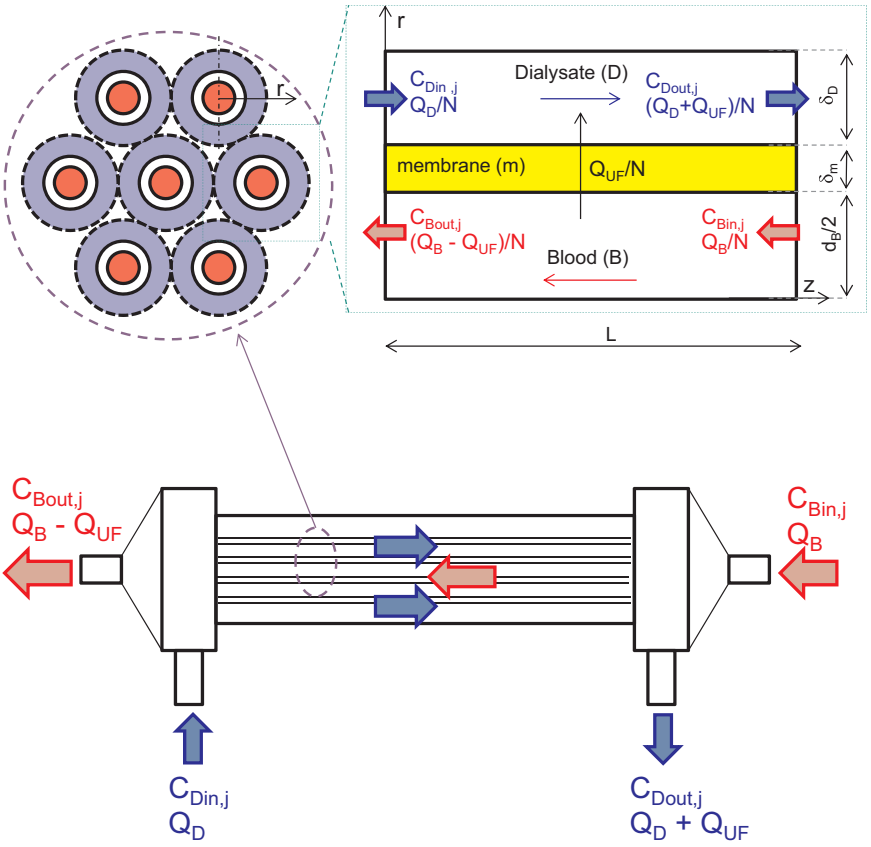

Fig. 1. Scheme of the hollow fiber dialyzer (lower panel) and how it is modeled in this study (upper panel).

lead to a decrease of the overall mass transfer coefficient in the dialysate compartment, resulting in a general worsening of dialyzer efficiency, due to the maldistribution of the dialysate flow rate therein. However, a partial compensation exists between the beneficial effects of the local increase of the dialysate flow rate in certain areas of the dialysate compartment and the detrimental effect of its local decrease in other areas, so that even the effect of a strong dialysate maldistribution on dialyzer efficiency may be generally tolerated [2,16]. The solutes considered are urea (molecular weight MW 60 Da), creatinine (MW 113 Da), phosphate (MW 95 Da), β_2-microglobuilin (MW 11000 Da) and myoglobin (MW16700 Da).

With reference to the dialyzer scheme in Fig. 1, the model assumptions are as follows:

i. axial symmetry
ii. flow in the blood and dialysate compartment is steady-state and laminar
iii. isothermal conditions (T = 37 °C)
iv. transport of momentum and mass occurs in 2D
v. incompressible fluids
vi. non-Newtonian behavior of blood is accounted for following Quemada et al. [17]
vii. Newtonian behavior of dialysate
viii. negligible effect of gravity
ix. momentum transport in the blood and dialysate compartments is described with the Navier-Stokes equations [18]
x. isotropic porous membrane consisting of a thin skin layer and a thick bulk layer [13]
xi. momentum transport in the membrane can be described using a pseudo-homogeneous approach with the Darcy-Brinkman equation [19]
xii. creeping flow in the membrane [13]
xiii. all membranes are exposed to the same boundary conditions, irrespective of their position in the bundle
xiv. strongly diluted solutes
xv. constant sieving coefficient
xvi. the effect of concentration polarization can be described with the film theory model [20]

Upon introducing the following non-dimensional coordinates and variables:

$$z^* = \frac{z}{L}\ ;\quad r^* = \frac{2r}{d_B}\ ;\quad u_i^* = \frac{u_i}{u_{B,in}}\ ;\quad v_i^* = \frac{2v_i}{u_{B,in}\, d_B/L}\ ;$$
$$P_i^* = \frac{4P_i}{u_{B,in}\,\mu_{B,in}\, L/{d_B}^2};\quad C_{i,j}^* = \frac{C_{i,j}}{C_{B,in,j}}\ ;$$
$$\rho_B^* = \frac{\rho_B}{\rho_{B,in}}\ ;\quad \mu_B^* = \frac{\mu_B}{\mu_{B,in}};\quad \pi^* = \frac{\pi}{\pi_0};\quad {C_p}^* = \frac{C_p}{C_{P,in}} \tag{1}$$

the governing conservation equations can be re-arranged in dimensionless form to give:

Continuity equation (i = B, m_s, m_b, D)

$$\frac{1}{r^*}\frac{\partial}{\partial r^*}(r^*\, {v_i}^*) + \frac{\partial {u_i}^*}{\partial z^*} = 0 \tag{2}$$

Blood side (B) - momentum balance equations

$$r)\quad \frac{u_{B,in} d_B \rho_{B,in}}{2\mu_{B,in}}\frac{d_B}{2L}{\rho_B}^*\left({v_B}^*\frac{\partial {v_B}^*}{\partial r^*} + {u_B}^*\frac{\partial {v_B}^*}{\partial z^*}\right)$$
$$= -\left(\frac{2L}{d_B}\right)^2\frac{\partial {P_B}^*}{\partial r^*} + {\mu_B}^*\frac{\partial}{\partial r^*}\left(\frac{1}{r^*}\frac{\partial}{\partial r^*}(r^*\, {v_B}^*)\right) + \left(\frac{d_B}{2L}\right)^2\frac{\partial^2 {v_B}^*}{\partial {z^*}^2} \tag{3}$$

$$z)\quad \frac{u_{B,in} d_B \rho_{B,in}}{2\mu_{B,in}}\frac{d_B}{2L}{\rho_B}^*\left({v_B}^*\frac{\partial {u_B}^*}{\partial r^*} + {u_B}^*\frac{\partial {u_B}^*}{\partial z^*}\right)$$
$$= -\frac{\partial {P_B}^*}{\partial z^*} + {\mu_B}^*\left(\frac{1}{r^*}\frac{\partial}{\partial r^*}\left(r^*\frac{\partial {u_B}^*}{\partial r^*}\right)\right) + \left(\frac{d_B}{2L}\right)^2\frac{\partial^2 {u_B}^*}{\partial {z^*}^2} \tag{4}$$

Membrane wall (m_λ) – momentum balance equations (λ = s, b)

$$r)\quad -\frac{k_{m,\lambda}L^2}{\delta_{m,\lambda}(d_B/2)^3}\frac{2\delta_{m,\lambda}}{d_B}\frac{\mu_{B,in}}{\mu_{m,\lambda}}\frac{\partial P_{m,\lambda}{}^*}{\partial r^*}+\frac{1}{\varepsilon_{m,\lambda}}\frac{k_{m,\lambda}}{(d_B/2)^2}\frac{\partial}{\partial r^*}\left(\frac{1}{r^*}\frac{\partial}{\partial r^*}(r^*\, v_{m,\lambda}{}^*)\right) - v_{m,\lambda}{}^* = 0 \tag{5}$$

$$z)\quad -\frac{k_{m,\lambda}}{(d_B/2)^2}\frac{\mu_{B,in}}{\mu_{m,\lambda}}\frac{\partial P_{m,\lambda}{}^*}{\partial z^*}+\frac{1}{\varepsilon_{m,\lambda}}\frac{k_{m,\lambda}}{(d_B/2)^2}\left[\frac{1}{r^*}\frac{\partial}{\partial r^*}\left(r^*\frac{\partial u_{m,\lambda}{}^*}{\partial r^*}\right)+\left(\frac{d_B}{2L}\right)^2\frac{\partial^2 u_{m,\lambda}{}^*}{\partial z^{*2}}\right]-u_{m,\lambda}{}^* = 0 \tag{6}$$

Dialysate side (D) - momentum balance equations

$$r)\quad \frac{u_{B,in}d_B\rho_{B,in}}{2\mu_{B,in}}\frac{d_B}{2L}\frac{\rho_D}{\rho_{\mathbf{B},in}}\frac{\mu_{B,in}}{\mu_D}\left(v_D{}^*\frac{\partial v_D{}^*}{\partial r^*}+u_D{}^*\frac{\partial v_D{}^*}{\partial z^*}\right) = -\left(\frac{2L}{d_B}\right)^2\frac{\partial P_D{}^*}{\partial r^*}+\frac{\partial}{\partial r^*}\left(\frac{1}{r^*}\frac{\partial}{\partial r^*}(r^*\, v_D{}^*)\right)+\left(\frac{d_B}{2L}\right)^2\frac{\partial^2 v_D{}^*}{\partial z^{*2}} \tag{7}$$

$$z)\quad \frac{u_{B,in}d_B\rho_{B,in}}{2\mu_{B,in}}\frac{d_B}{2L}\frac{\rho_D}{\rho_{\mathbf{B},in}}\frac{\mu_{B,in}}{\mu_D}\left(v_D{}^*\frac{\partial u_D{}^*}{\partial r^*}+u_D{}^*\frac{\partial u_D{}^*}{\partial z^*}\right) = -\frac{\partial P_D{}^*}{\partial z^*}+\left(\frac{1}{r^*}\frac{\partial}{\partial r^*}\left(r^*\frac{\partial u_D{}^*}{\partial r^*}\right)\right)+\left(\frac{d_B}{2L}\right)^2\frac{\partial^2 u_D{}^*}{\partial z^{*2}} \tag{8}$$

Eqs. (1)–(8) may be solved with the following boundary conditions: fiber axis and dialysate-side outer boundary impervious to momentum and fluid (i.e. $\forall z^*$ at $r^* = 0$ and $r^* = (1 + 2\delta_m/d_B + 2\delta_D/d_B)$, $\partial u_i{}^*/\partial r^* = 0$ and $v_i{}^* = 0$, i = B, D); fully developed velocity profile at the blood and dialysate entrances; continuity of axial and radial velocity at blood-membrane and membrane-dialysate interfaces and at the interface between membrane skin and bulk layers; continuity in pressure at membrane-dialysate interface and at the interface between membrane skin and bulk layers; interfaces at the end sections of the membrane impervious to momentum and fluid (i.e. at $1 < r^* < (1 + 2\delta_{m,s}/d_B)$ and $(1 + 2\delta_{m,s}/d_B) < r^* < (2\delta_{m,s}/d_B + 2\delta_{m,b}/d_B + 1)$, at $z^* = 0$ and $z^* = 1$, $u_{m,\lambda}{}^* = 0$, λ = b, s); constant pressure at blood and dialysate-sides exits. Assuming the plasma proteins to be completely rejected by the membrane, the oncotic pressure (i.e. the osmotic pressure exerted by the plasma proteins), was implemented as a discontinuous pressure drop at the interface between the blood compartment and membrane skin wall (i.e. $\forall z^*$ at $r^* = 1$, $P_{m,s}{}^* = P_B{}^* - \pi_0{}^*\pi^*$), and calculated according to the correlation proposed by Landis and Pappenheimer [21] as:

$$\pi^* = C_{p,in}\frac{\pi_1}{\pi_0}C_{p,w}{}^* + C_{p,in}{}^2\frac{\pi_2}{\pi_0}C_{p,w}{}^{*2} + C_{p,in}{}^3\frac{\pi_3}{\pi_0}C_{p,w}{}^{*3} \tag{9}$$

where $\pi_1 = 0.21$ mmHg l/g, $\pi_2 = 1.6 \times 10^{-3}$ mmHg l^2/g^2, $\pi_3 = 9 \times 10^{-6}$ mmHg l^3/g^3.

The protein concentration at the blood-membrane skin interface was computed according to the film theory model [20] as:

$$C_{p,w}{}^* = C_p{}^* \exp(v_{B|r=dB/2}/k_{c,p}) \tag{10}$$

The concentration of the completely rejected protein varies with the local flow rate as

$$\frac{d(Q_B(z)/Q_B C_p{}^*)}{dz^*} = 0 \tag{11}$$

with $C_p{}^* = 1$ at $z^* = 0$. The mass transfer coefficient, which varies with the axial coordinate, was computed from the Sherwood number as

$$Sh_p = 1.62\left(\mathrm{Re}_{B,p}Sc_{B,p}\frac{d_B}{z}\right)^{1/3} = \frac{k_{c,p}d_B}{D_{B,p}} \tag{12}$$

where

$$\mathrm{Re}_{B,p} = \frac{u_{in,B}d_B\rho_{B,in}}{\mu_{B,in}};\quad Sc_B = \frac{\mu_{B,in}}{\rho_{B,in}D_{B,p}} \tag{13}$$

In Eq. (3), blood viscosity was assumed to vary in both radial and axial direction. In particular, the shear thinning behavior and the dependence of blood viscosity on the local hematocrit were described according to the model reported by Quemada [17].

Mass conservation for a j-th solute (j = urea, creatinine, phosphate, β_2-microglobulin, myoglobin):

Blood side – convection-diffusion equation

$$\frac{u_{B,in}L}{D_{B,j}}\left(\frac{d_B}{2L}\right)^2\left(v_B{}^*\frac{\partial C_{B,j}{}^*}{\partial r^*}+u_B{}^*\frac{\partial C_{B,j}{}^*}{\partial z^*}\right) = \frac{1}{r^*}\frac{\partial}{\partial r^*}\left(r^*\frac{\partial C_{B,j}{}^*}{\partial r^*}\right)+\left(\frac{d_B}{2L}\right)^2\frac{\partial^2 C_{B,j}{}^*}{\partial z^{*2}} \tag{14}$$

Membrane (λ = s, b) – convection-diffusion equation

$$\frac{u_{B,in}L}{D_{B,j}}\left(\frac{d_B}{2L}\right)^2\frac{D_{B,j}}{D_{m,\lambda,j}}S_j\left(v_{m,\lambda}{}^*\frac{\partial C_{m,\lambda,j}{}^*}{\partial r^*}+u_{m,\lambda}{}^*\frac{\partial C_{m,\lambda,j}{}^*}{\partial z^*}\right) = \frac{1}{r^*}\frac{\partial}{\partial r^*}\left(r^*\frac{\partial C_{m,\lambda,j}{}^*}{\partial r^*}\right)+\left(\frac{d_B}{2L}\right)^2\frac{\partial^2 C_{m,\lambda,j}{}^*}{\partial z^{*2}} \tag{15}$$

Dialysate side – convection-diffusion equation

$$\frac{u_{B,in}L}{D_{B,j}}\left(\frac{d_B}{2L}\right)^2\frac{D_{B,j}}{D_{D,j}}\left(v_D{}^*\frac{\partial C_{D,j}{}^*}{\partial r^*}+u_D{}^*\frac{\partial C_{D,j}{}^*}{\partial z^*}\right) = \frac{1}{r^*}\frac{\partial}{\partial r^*}\left(r^*\frac{\partial C_{D,j}{}^*}{\partial r^*}\right)+\left(\frac{d_B}{2L}\right)^2\frac{\partial^2 C_{D,j}{}^*}{\partial z^{*2}} \tag{16}$$

Eqs. (14)–(16) were solved with the following boundary conditions: uniform and zero solute concentration profile in the stream entering the blood and the dialysate compartments, respectively; fiber axis and dialysate-side outer boundary impervious to mass (i.e. $\forall z^*$ at $r^* = 0$ and $r^* = (1 + 2\delta_m/d_B + 2\delta_D/d_B)$, $\partial C_{i,j}{}^*/\partial r^* = 0$, i = B, D); continuous solute concentrations and mass fluxes at the interfaces of neighboring regions; interfaces at the end sections of the membrane impervious to mass (i.e. at $1 < r^* < (2\delta_{m,s}/d_B + 1)$ and $(1 + 2\delta_{m,s}/d_B) < r^* < (2\delta_{m,s}/d_B + 2\delta_{m,b}/d_B + 1)$, at $z^* = 0$ and $z^* = 1$, $\partial C_{m,\lambda,j}{}^*/\partial z^* = 0$, λ = b, s); solute concentrations in the streams leaving blood and dialysate compartments do not change any further (i.e. at $0 < r^* < d_B/2$, $z^* = 1$ and at $(1 + 2\delta_m/d_B) < r^* < (1 + 2\delta_m/d_B + 2\delta_D/d_B)$, $z^* = 0$, $\partial C_{i,j}{}^*/\partial z^* = 0$, i = B, D).

2.2. Dimensionless groups

Analysis of Eqs. (1)–(16) and related boundary conditions shows that dialyzer efficiency is determined by the values of the independent dimensionless groups reported in Table 1. Such dimensionless groups account for module geometry, properties of the fluids, membrane properties, operating conditions and solute properties. The physical meaning of most of them has previously been reported in the literature [18,22,23]. In particular, the value of α, which accounts for the ability of the membrane to enable ultrafiltration for given pressure drops in the blood and dialysate compartments, was kept in the range reported for low and high flux ultrafiltration membranes, typically adopted in hemodialysis. The product between the j-th maximal axial Peclet number at the blood-side inlet, $Pe_{ax,\ B,\ max,\ j} = u_{in,B}L/D_{B,j}$, and the squared membrane shape ratio, $d_B/(2\,L)$, is referred to as the maximal reduced Peclet number, $Pe_{r,\ max,\ j}$, and provides a measure of the relative importance of convective-to-diffusive solute transport along the radial coordinate at a given membrane pressure modulus. In the simulations, the Reynolds number at the blood-side inlet, Re_B, and the dialysate-to-blood flow rate ratio, Q_D/Q_B, were kept in the range used in clinical practice to enable laminar flow, thus justifying the use of the Navier–Stokes equation.

Finally, the effect of the membrane thickness-to-fiber inner radius ratio, $2\delta_m/d_B$, and the dialysate-side thickness-to-fiber inner radius ratio, $2\delta_D/d_B$, was better evaluated in terms of the module packing density, defined as:

Table 1
Dimensionless groups determining dialyzer performance.

Dimensionless group	Description
1. $u_{in,B}d_B\rho_{B,in}/(2\mu_{B,in}) = Re_B$	Reynolds number at blood-side inlet
2. $2L/d_B$	Fiber aspect ratio
3. $(128k_mL^2/(d_B{}^3\delta_m))^{1/2} = \alpha$	Membrane pressure modulus
4. $2\delta_m/d_B$	Membrane thickness-to-fiber inner radius ratio
5. $\mu_{B,in}/\mu_{m,\lambda}$	Blood-to-membrane λ-th layer side viscosity ratio
6. μ_{Bin}/μ_D	Blood-to-dialysate side viscosity ratio
7. $\rho_D/\rho_{B,in}$	Dialysate-to-blood density ratio
8. $2\delta_D/d_B$	Dialysate side thickness-to-fiber inner radius ratio
9. Q_D/Q_B	Dialysate-to-blood side inlet flow rate ratio
10. $4\pi_0 d_B{}^2/(\mu_{B,in}u_{in,B}L) = \pi_0{}^*$	Dimensionless oncotic pressure
11. $u_{in,B}L/D_{B,j}\ (d_B/(2L))^2 = Pe_{r,max,j}$	Maximal reduced Peclet number of the j-th solute
12. $D_{B,j}/D_{m,j}$	Blood-to-membrane j-th solute diffusivity ratio
13. $D_{B,j}/D_{D,j}$	Blood-to-dialysate j-th solute diffusivity ratio
14. $2k_{c,p}/(u_{in,B}d_B/L)$	Dimensionless mass transfer coefficient at B-m interface

$$PD = \frac{4N(d_B/2 + \delta_m)^2}{d_H{}^2} = \left(\frac{1 + \frac{2\delta_m}{d_B}}{1 + \frac{2\delta_m}{d_B} + \frac{2\delta_D}{d_B}}\right)^2 = f(\delta_D/d_B,\ \delta_m/d_B) \tag{17}$$

2.3. Computational methods

Model Eqs. (1)–(16) and related boundary conditions were integrated numerically with the commercial Finite Element Method Code Comsol Multiphysics (Comsol Inc., Burlington, MA, USA). The spatial domain was discretized with a non-uniform mesh of more than 400,000 rectangular elements. Local mesh refinement was applied to integrate model equations in the blood and membrane compartments, due to the higher complexity of the model equations therein, at blood and dialysate inlets and outlets, and at the membrane interfaces with blood and dialysate compartments. The minimal number of the mesh elements and their distribution in the integration domain were optimized for each set of dimensionless groups to keep the relative error on the predicted solute mixing cup concentrations at blood- side outlet below 0.005%. Two-dimensional steady-state profiles of dimensionless axial and radial velocity, pressure, and solute concentrations were found for values of model parameters and dimensionless groups typically reported for dialysis applications listed in Table 2a and 2b unless otherwise specified. In particular, in order to account for the fiber curvature, the overall membrane Darcy permeability was calculated from the hydraulic permeability as [27]

$$k_m = L_p \frac{\mu_m}{\varepsilon_m}\frac{d_B}{2}\log\frac{\frac{d_B}{2} + \delta_m}{\frac{d_B}{2}} \tag{18}$$

where

$$L_p = \frac{K_{UF}}{A_{tot}} \tag{19}$$

The dialyzer efficiency was assessed in terms of dimensionless solute clearances, calculated as [28,29]

$$Cl_j{}^* = \frac{Cl_j}{Q_B} = \frac{C_{B,in,j} - C_{B,out,j}}{C_{B,in,j}} + S_j\frac{Q_{UF}}{Q_B} \tag{20}$$

2.4. Model validation

The model was validated by comparing model-predicted clearances of each solute to corresponding experimental data reported in literature obtained by operating dialyzer modules at increasing blood and dialysate flow rates. Due to the lack of comprehensive datasets of solute diffusivities for each dialyzer membrane, solute diffusivities in the membrane were found iteratively until model-predicted solute clearances matched the experimental data, assuming blood and dialysate–sides diffusivities reported in Table 2. In accordance with the available experimental results used for model validation, solute clearances were calculated from the dialysate flow rate as [26]:

$$Cl_j = (Q_D + Q_{UF})\frac{C_{D,out,j}}{C_{pl,in,j}} \tag{21}$$

3. Results and discussion

The model proposed in this paper aims to investigate how geometric, transport and operating parameters affect solute clearance, and to provide a framework that permits the adjustment of such parameters in order to maximize solute clearances, so that newly designed dialyzers may be realized in a cost-effective way. In fact, no model reported in the literature was able to perform an in-depth analysis of all the dimensionless groups determining solute clearance, nor to find design criteria for dialyzer optimization.

3.1. Model validation

Figs. 2a and b show the comparison between model-predicted and in vivo solute clearances obtained with Theranova 400 MCO AA (Gambro Dialysatoren GmbH, Germany, a subsidiary of Baxter International Inc.) (Fig. 2a) and FX CorDiax 80 (Fresenius Medical Care, Bad Homburg, Germany) (Fig. 2b), at increasing blood flow rates. Furthermore, Fig. 2c shows the comparison between model-predicted and in vivo solute clearances obtained with FX CorDiax 800 (Fresenius Medical Care, Bad Homburg, Germany), operated in hemodiafiltration. The clinical data are reported in Kirsch et al. [24]. In all cases, good agreement between model-predicted and in vivo clearances was found at any blood flow rate for each solute, independent of solute molecular

Table 2a
Model parameter values used for model predictions.

Parameter	Value	Unit	Reference
L	23	cm	[13]
d_B	200	μm	[13]
$\delta_{m,\lambda}$	1 (λ = s), 34 (λ = b)	μm	[13]
d_H	38	mm	[24]
N	12960	–	[24]
H_{in}	0.3	–	[13]
μ_{pl}	1.3×10^{-3}	Pa s	[22]
$C_{p,in}$	58	g/l	[24]
ρ_D	1008	kg/m^3	[13]
μ_D	0.687×10^{-3}	Pa s	[13]
K_{UF}	48	ml/h/mmHg	[24]
$\varepsilon_{m,s}$, $\varepsilon_{m,b} = \varepsilon_m$	0.8	–	
Q_{UF}	0–30	ml/min	[3]
Q_B	200–500	ml/min	[13]
Q_D	500	ml/min	[25]
$D_{B,j}$	17.5×10^{-10} (urea), 2.57×10^{-10} (phosphate), 7.9×10^{-10} (creat), 1.18×10^{-10} (β_2m), 1.05×10^{-10} (myo)	m^2/s	[13,22]
$D_{m,j}$	1.9×10^{-10} (urea), 2.5×10^{-10} (phosphate), 9.5×10^{-11} (creat), 5.9×10^{-11} (β_2m), 3.75×10^{-11} (myo)	m^2/s	[13,24,26]
$D_{D,j}$	19×10^{-10} (urea), 2.67×10^{-10} (phosphate), 9.66×10^{-10} (creat), 2.09×10^{-10} (β_2m), 1.85×10^{-10} (myo)	m^2/s	[13,22]
S_j	1 (j = urea, creat, phosphate, β_2m); 0.9 (j = myo)	–	[13,24]

Table 2b
Dimensionless groups values used for model predictions.

Dimensionless group	Value
1. uin,BdBρB,in/(2μB,in) = ReB	0.56–1.4
2. 2 L/dB	2300
3. (128 kmL2/(dB3δm))1/2 = α	0.22
4. 2δm/dB	0.35
5. μB,in/μm	1.35
6. μBin/μD	2.55
7. ρD/ρB,in	0.95
8. 2δD/dB	0.32
9. QD/QB	1–2.5
10. π0dB2/(2μB,inuin,BL)	3.68
11. uin,BL/DB,j(dB/(2 L))2 = Per,max,j	0.1–0.75 (urea); 1.75–12.5 (myo); 0.5–5 (phosphate); 0.2–1.7 (creat); 1.6–10.8 (β2m)
12. Dm,j/DB,j	0.11 (urea); 0.35 (myo); 0.97 (phosphate); 0.12 (creat); 0.5 (β2m)
13. DD,j/DB,j	1.1 (urea); 1.76 (myo); 0.96 (phosphate); 1.22 (creat); 1.77 (β2m)
14. 2kc,p/(uindB/L)	0.06–0.11

weight. Fig. 2d shows that good agreement between model-predicted and in vivo clearances of urea, phosphate, and β_2-microglobulin was also found for the Revaclear Max (Gambro Dialysatoren GmbH, Germany, a subsidiary of Baxter International Inc.) dialyzer (experimental data reported in Bhimani et al. [30]), at increasing dialysate flow rates. In particular, the percentage error between model-predicted and in vivo clearance is lower than 7% for each solute at any simulated condition. The values of the solute membrane diffusivities that best fitted the in vivo data are reported in Table 3.

3.2. Effect of dimensionless groups on solute clearance

Table 1 shows that the dialyzer efficiency is determined by fourteen independent dimensionless groups. In particular, the membrane pressure modulus, α, mainly accounting for membrane transport properties; the Reynolds number at blood inlet, Re_B, and the dialysate-to-blood flow rate ratio, Q_D/Q_B, mainly accounting for the extent of blood and dialysate flow rates, respectively; the dimensionless pressure at blood and dialysate-side exits, P_{Bout}^* and P_{Dout}^*, mainly accounting for the extent of the ultrafiltration flow rate, Q_{UF}; the fiber aspect ratio, L/d_B, and the module packing density, $PD = f(2\delta_m/d_B, 2\delta_D/d_B)$, accounting for module geometry. In this section, the influence of this set of dimensionless groups on solute clearance is discussed.

Table 3
Solute membrane diffusivities $D_{m,j}$ (m^2/s) best fitting the in vivo solute clearances.

Filter	$D_{m,urea}$	$D_{m,creat}$	$D_{m,PO4}$	$D_{m,β2-m}$	$D_{m,myo}$
Theranova 400 AA	2.6×10^{-10}	9.5×10^{-11}	2.5×10^{-10}	–	3.75×10^{-11}
FX CorDiax 80	2.4×10^{-10}	1.2×10^{-10}	2.3×10^{-10}	–	8×10^{-12}
FX CorDiax 800	2.6×10^{-10}	8.2×10^{-11}	1.2×10^{-10}	–	1×10^{-11}
Revaclear MAX	4.8×10^{-10}	–	1.5×10^{-10}	5.9×10^{-11}	–

3.2.1. Effect of membrane pressure modulus on solute clearance

Fig. 3a shows the effect of the membrane pressure modulus, α, on solute clearance at given module geometry and operating conditions. At lower values of α, membrane resistance is high and solutes are mainly transported by diffusion. This causes the solute clearance to be quasi-independent of the membrane pressure modulus. As the membrane pressure modulus increases for constant axial pressure drop in the blood and dialysate compartments, convective transport across the membrane is enhanced by the decreasing resistance to mass transport therein, which increases the forward ultrafiltration flow rate across the membrane (Fig. 3b) and causes a slight increase of the solute clearances. This effect is slightly more evident for middle molecular weight solutes (i.e. myoglobin and β_2-microglobulin). However, the increase of solute clearance for higher membrane pressure moduli at given Q_{UF} shown in Fig. 3a is low for each solute, so that the effect of the pressure modulus on solute clearances may be actually considered negligible. This is likely due to the fact that the solute diffusivities in the membrane were kept constant for varying values of the pressure modulus.

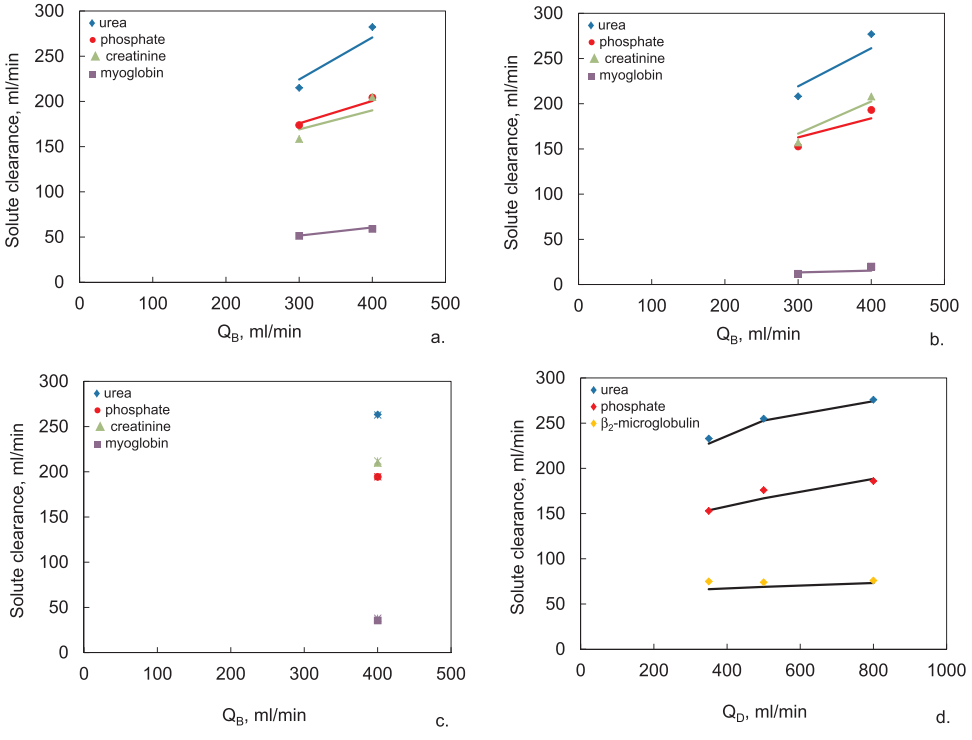

Fig. 2. Model-predicted (solid lines) vs. in vivo (symbols) solute clearances for: a) Theranova 400 MCO AA, model parameters as in Kirsch et al. [24]; b) FX CorDiax 80, model parameters as in Kirsch et al. [24]; c) FX CorDiax 800, model parameters as in Kirsch et al. [24]; d) Revaclear Max, model parameters as in Bhimani et al. [30].

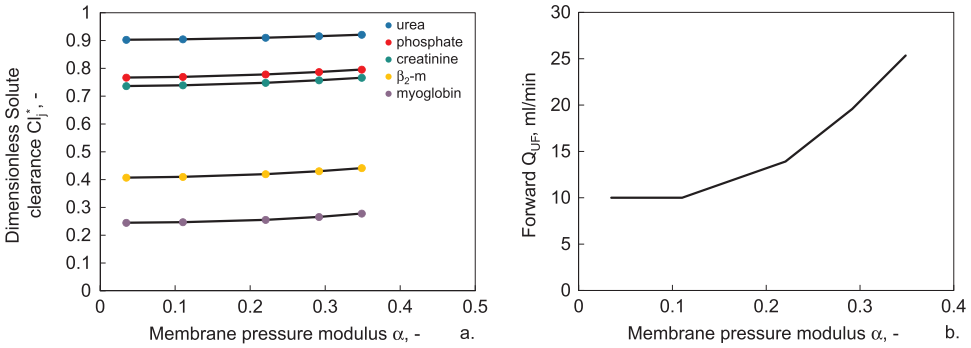

Fig. 3. Effect of membrane pressure modulus, α, at Q_{UF} = 10 ml/min, L/d_B = 1150, PD = 0.65, Q_D/Q_B = 1, on a) dimensionless solute clearances and b) forward ultrafiltration flow rate. Model parameters as in Tables 1 and 2.

3.2.2. *Effect of module geometry on solute clearance*

Figs. 4 and 5 show the effect of module geometry on dimensionless solute clearances at constant membrane pressure modulus and operating conditions. Fig. 4 shows the effect of the fiber aspect ratio, 2 L/d_B, on solute clearances. For each solute, dimensionless clearance increases with fiber aspect ratio. For low molecular weight solutes, dimensionless clearance increases up to a plateau (i.e. up to $Cl_j^* = 1$). Since the membrane pressure modulus is kept constant, the increasing solute clearance with increasing L/d_B has to be completely attributed to the increasing total module surface area. Fig. 5a shows the effect of the module packing density, PD, on the dimensionless solute clearances. For each solute, dimensionless clearance increases as the module packing density increases. This result is consistent with literature data [31]. This effect is mostly due to the increasing total module surface area. In fact, Fig. 5b shows that the effect of the module packing density on the dimensionless clearance of urea and myoglobin becomes quasi negligible if the total surface area and the membrane pressure modulus are both kept constant, although a slight increase of dimensionless clearance may be noticed for high packing densities where the pressure drop in the dialysate compartment increase.

3.2.3. *Effect of operating conditions on dimensionless solute clearances*

Fig. 6 shows the effect of the operating conditions on dimensionless solute clearances at given geometry and membrane transport properties. Fig. 6a shows that the dimensionless clearance generally increases as the net ultrafiltration flow rate (i.e. the difference between the forward and the backward ultrafiltration flow rate), Q_{UF}, increases, for each solute. The dependence of the dimensionless clearance on Q_{UF} strongly depends on the molecular weight of the solute. In fact, the dimensionless clearance of the low molecular weight solutes (i.e. urea, creatinine and phosphate) depends slightly on Q_{UF}. This is explained by the fact that, due to its high diffusivity across the membrane wall and in the fluid compartments, transport of urea mainly occurs by diffusion. The effect of the net ultrafiltration flow rate, Q_{UF}, on the dimensionless clearance increases for middle molecular weight solutes (i.e. β_2-m and myoglobin). This is explained by the fact that, due to their higher molecular weight and lower diffusivity across the membrane wall and in the fluid compartments, transport of middle molecular weight solutes is enhanced by convection. Furthermore, Fig. 6a shows that the dimensionless solute clearance generally increases as the dialysate-to-blood flow rate ratio, Q_D/Q_B, increases. This effect is more evident for low molecular weight solutes. This is justified by the fact that, for low molecular weight solutes, at constant blood flow rate (i.e. constant Re_B), an increase of the dialysate flow rate makes the resistance to solute transport from the membrane wall towards the dialysate bulk decrease. On the other hand, the low diffusivity of middle molecular weight solutes across the membrane wall makes transport across the membrane limiting for their removal, so that an increase of Q_D/Q_B at constant Re_B has a negligible effect on the dimensionless clearance. Fig. 6b shows that, at constant Q_D/Q_B, an increase of the blood flow rate (i.e. an increase of Re_B) leads to a decrease in transport solute resistance, resulting in an increase of solute clearances (in absolute value). However, since the increase of solute clearance for increasing blood flow rate is less than linear, the dimensionless solute clearance decreases for increasing Re_B.

3.3. *Unifying approach to dialyzer optimization*

Dimensional analysis shows that a more apt dimensionless group to assess the enhancement of solute transport (i.e. the solute clearances) is the maximal j-th reduced Peclet number, $Pe_{r,max,j}$. In the sections above, we already presented some of our results in terms of dimensionless numbers, which combine and integrate the effect of individual variables. Further expanding the dimensional analysis, it can be shown that the dimensionless group that best expresses the solute transport - and hence allows assessing the enhancement in solute clearance – is the maximal j-th reduced Peclet number, $Pe_{r,max,j}$.

Fig. 7 shows that, when the values of the dimensionless solute clearances are rearranged vs. $Pe_{r,\ max,j}$, all curves reported in Figs. 3–6 converge towards one curve only for a constant value of Q_D/Q_B and for a given solute. This suggests that the maximal reduced Peclet number accounts well for the effect of the most relevant dimensionless groups determining solute transport. This observation is also supported by results reported by Ward and Ouseph [32] on the clearance of urea, phosphate, and β_2-microglobulin determined experimentally with Polyflux 210H and Revaclear Max dialyzers (Gambro Dialysatoren GmbH, Germany, a subsidiary of Baxter International Inc.) operated at the same working conditions (Fig. 8). At the same operating conditions, the authors report an equivalent dialyzer performance for the two dialyzer modules over the wide range of solute molecular weights, despite their significantly different geometry.

In particular, urea, phosphate and β_2-microglobulin clearances have been reported to be equal to around 296, 169 and 121 ml/min, respectively, for Polyflux 210 H (A_{tot} = 2.1 m^2, d_B = 215 μm, δ_m = 50 μm, PD = 0.45) and 295, 184 and 126 ml/min, respectively, for Revaclear Max (A_{tot} = 1.8 m^2, d_B = 190 μm, δ_m = 35 μm, PD = 0.56), both operated at Q_B = 400 ml/min, Q_D = 800 ml/min and Q_{UF} = 0 ml/min. These conditions yield $Pe_{r,\ max,\ urea}$ = 0.43, $Pe_{r,\ max,\ PO4}$ = 2.93 and $Pe_{r,max,\beta2\text{-}m}$ = 15.89 for Polyflux 210 H and $Pe_{r,max,urea}$ =

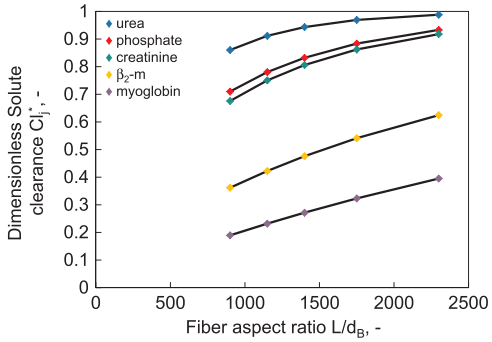

Fig. 4. Effect of fiber aspect ratio, 2 L/d_B, at Q_{UF} = 10 ml/min, α = 0.22, PD = 0.65, Q_D/Q_B = 1, on dimensionless solute clearances. Model parameters as in Tables 1 and 2.

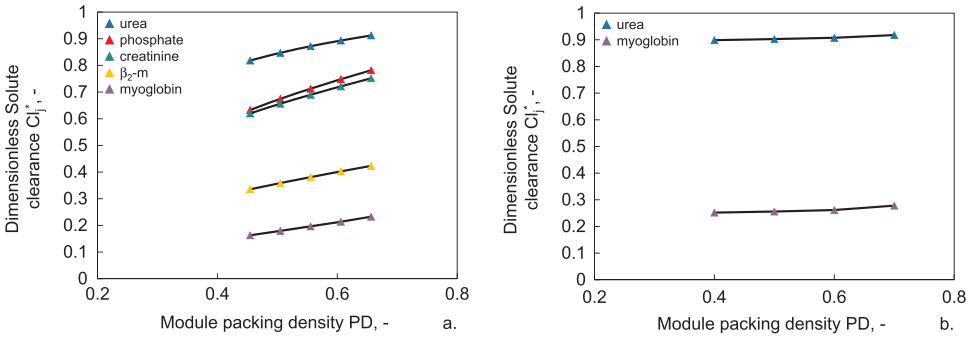

Fig. 5. Effect of module packing density, PD, at Q_{UF} = 10 ml/min, Q_D/Q_B = 1, on a) dimensionless solute clearances at α = 0.22 and L/d_B = 1150 and b) dimensionless urea and myoglobin clearance at α = 0.22 and A_{tot} = 1.9 m^2. Model parameters as in Tables 1 and 2.

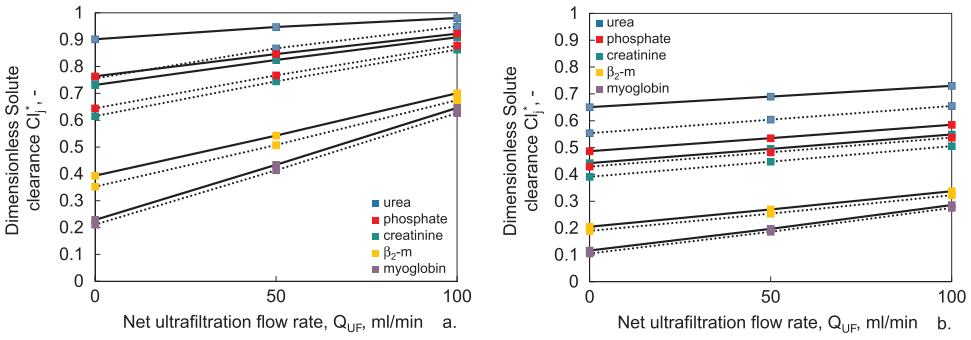

Fig. 6. Effect of operating conditions at α = 0.22, L/d_B=1150, PD = 0.65, on dimensionless solute clearance at Q_D/Q_B = 1 (···) and Q_D/Q_B = 2.5 (—) for a) Re_B = 0.56 and b) Re_B = 1.4. Model parameters as in Tables 1 and 2.

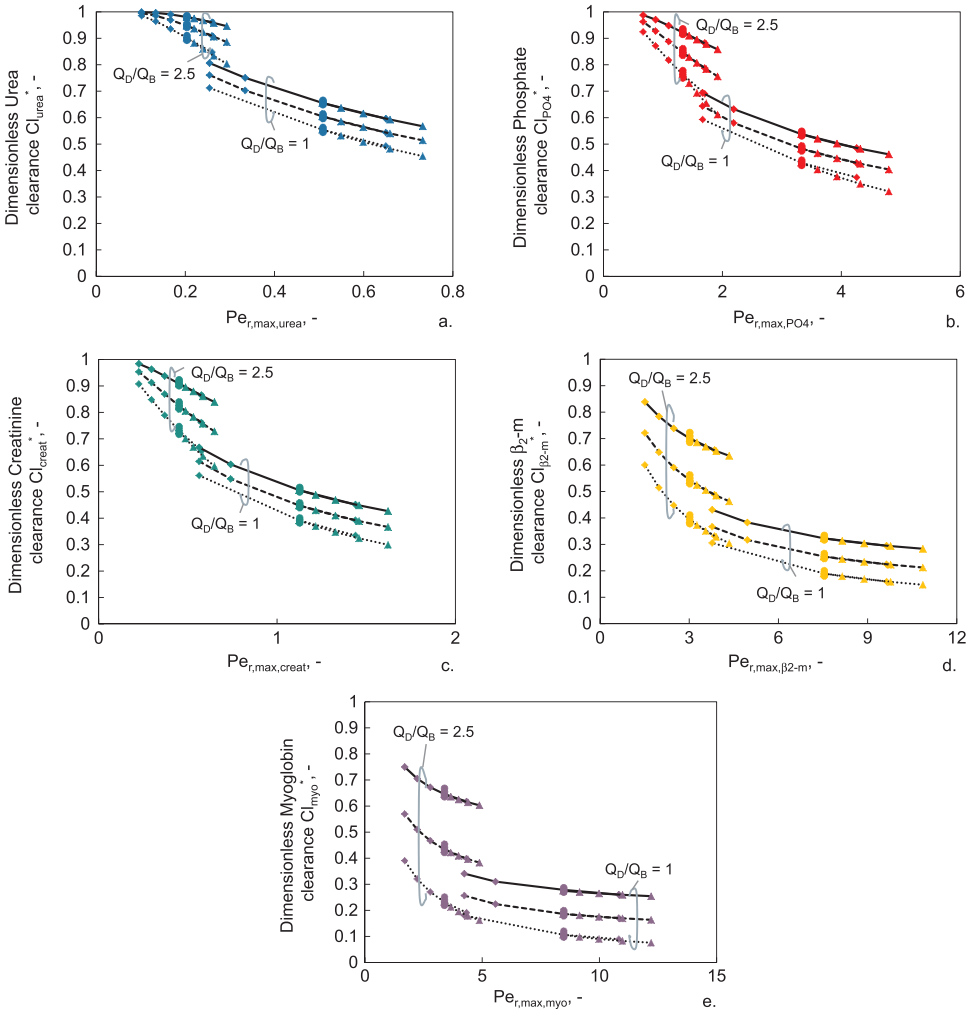

Fig. 7. Effect of maximal reduced Peclet number, $Pe_{r,max,j}$ and dialysate-to-blood flow rate ratio, Q_D/Q_B, on dimensionless clearance of a) urea, b) phosphate, c) creatinine, d) β_2-microglobulin, e) myoglobin for Q_{UF} = 0 ml/min (···), Q_{UF} = 50 ml/min (- - -), Q_{UF} = 100 ml/min (—). • L/d_B = 1150, PD = 0.65; ▲α = 0.22, L/d_B = 1150; ♦ α = 0.22, PD = 0.65. Other parameters as in Tables 1 and 2.

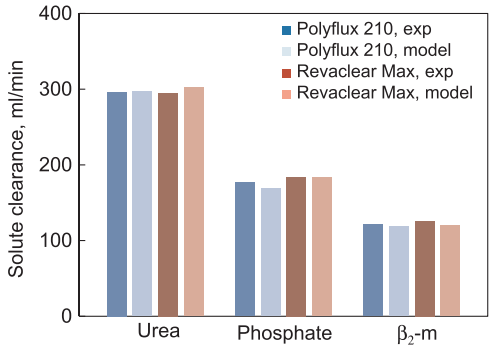

Fig. 8. Model-predicted vs. experimental clearances of urea, phosphate and β_2-microglobulin obtained with Gambro modules Polyflux 210 H and Revaclear Max. Model parameters as in Ward and Ouseph [32].

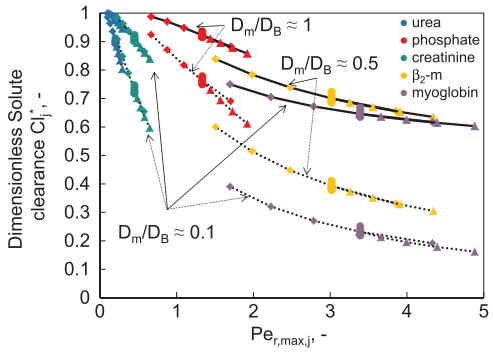

Fig. 9. Effect of maximal reduced Peclet number, $Pe_{r,max,j}$ and membrane-to-blood j-th solute diffusivity ratio $D_{m,j}/D_{B,j}$ on dimensionless solute clearance at $Q_D/Q_B = 1$ for $Q_{UF} = 0$ ml/min (···), $Q_{UF} = 100$ ml/min (—). • L/d_B = 1150, PD = 0.65; ▲α = 0.22, L/d_B = 1150; ◆ α = 0.22, PD = 0.65. Other parameters as in Tables 1 and 2.

0.43, $Pe_{r,max,\ PO4} = 2.92$ and $Pe_{r,max,\beta2\text{-}m} = 15.88$ for Revaclear Max.

The maximal reduced Peclet number does not depend on any parameter related to intrinsic membrane transport properties (e.g. membrane permeability, solute diffusivity across the membrane), but only on membrane geometry and operating conditions. This, on the one hand, implies that this parameter is not directly an alternative for the currently used dialyzer classification. On the other hand, it has the advantage that it can be used to optimize the overall design of dialyzers – and their operating conditions - independent of their classification (e.g. low or high –flux)

Fig. 7 also suggests that dimensionless clearance may be maximized by minimizing the value of the maximal reduced Peclet number for a given value of Q_B/Q_D. Furthermore, Fig. 7 shows that the net ultrafiltration flow rate, Q_{UF}, has a less important influence on the dimensionless clearance of urea (Fig. 7a), phosphate (Fig. 7b) and creatinine (Fig. 7c) than on the dimensionless clearance of β_2-microglobulin (Fig. 7d) and myoglobin (Fig. 7e).

Fig. 9 shows that the dimensionless solute clearance also depends on the membrane-to-blood side solute diffusivity ratio, $D_{m,j}/D_{B,j}$. In fact, all the curves related to urea, creatinine and myoglobin, for which $D_{m,j}/D_{B,j} \approx 0.1$, converge in one curve only for constant Q_D/Q_B, whereas those related to β_2-microglobulin and phosphate, for which $D_{m,j}/D_{B,j} \approx$ 0,5 and 1, respectively, are shifted towards higher dimensionless clearances. Fig. 9 also evidences that the effect of Q_{UF} increases as the maximal reduced Peclet number increases.

4. Conclusions

The results reported in this work suggest that dialyzer efficiency depends on the interplay among geometrical, membrane-related and operational parameters. These parameters can be combined into dimensionless groups, found by dimensional analysis, determining momentum and mass transport in all the compartments of the dialyzer. A novel approach to design optimized dialyzers, accounting for the effect of all the dimensionless groups determining solute transport in the dialyzer, was developed in this paper. We demonstrated that solute clearances may be maximized in a cost-effective way by designing dialyzer geometry such that the solute maximal reduced Peclet number, which accounts for the relative importance of convective and diffusive solute transport, is minimized for constant dialysate-to-blood flow rate ratios. An important advantage of the design approach presented in this paper is that it can be used for the optimization of low and high –flux dialyzers. Furthermore, experimental literature results show that the approach presented in this paper may be extended to the removal of both small and middle sized molecules. Dialyzer design matching the results presented in this paper allows for dialyzer scale-up in order to reduce the blood contact area and the blood-side volume, as well as the amount of medical waste, while ensuring adequate solute removal for blood purification.

Conflict of interests

DD, AB, CZ, MK, MS and BK are employees of Gambro Dialysatoren GmbH, 72379 Hechingen, Germany. Gambro AB (including all direct and indirect subsidiaries) is part of Baxter International Inc. All other authors declare that they do not have conflict of interest.

Acknowledgements

This work was conducted within the context of a research project funded by Gambro Dialysatoren GmbH, Germany, a subsidiary of Baxter International Inc.

References

[1] J.E. Sigdell, Calculation of combined diffusive and convective mass transfer, Int. J. Artif. Organs 5 (1982) 361–372.
[2] C. Vander Velda, E.F. Leonard, Theoretical assessment of the effect of flow maldistributions on the mass transfer efficiency of artificial organ, Med. Biol. Eng. Comp. 23 (1985) 224–229.
[3] C. Legallais, G. Catapano, B. von Harten, U. Baurmeister, A theoretical model to predict the in vitro performance of hemodiafilters, J. Mem. Sci. 168 (2000) 3–15.
[4] T. Kunimoto, E.G. Lowrie, Kumazawa, et al., Controlled ultrafiltration (UF) with hemodialysis (HD): analysis of coupling between convective and diffusive mass transfer in a new HD-UF system, Trans. ASAIO 23 (1977) 234–241.
[5] M.Y. Jaffrin, B.B. Gupta, J.M. Malbrancq, A one-dimensional model of simultaneous hemodialysis and ultrafiltration with highly permeable membranes, J. Biomech. Eng. 103 (1981) 261–266.
[6] Y.L. Chang, C.J. Lee, Solute transport characteristics in hemodiafiltration, J. Membr. Sci. 39 (1988) 99–111.
[7] A. Werynski, J. Wanieski, Theoretical description of mass transport in medical membrane devices, Artif. Organs 19 (5) (1995) 420–427.
[8] A. Wüpper, D. Woermann, F. Dellanna, C.A. Baldamus, Retrofiltration rates in high-flux hollow fiber hemodialysers: analysis of clinical data, J. Membr. Sci. 121 (1996) 109–116.
[9] A. Wüpper, F. Dellanna, C.A. Baldamus, D. Woermann, Local transport processes in high-flux hollow fiber dialyzers, J. Membr. Sci. 131 (1997) 181–193.
[10] M. Raff, M. Welsch, H. Göhl, H. Hildwein, M. Storr, B. Wittner, Advanced modeling of high flux hemodialysis, J. Mem. Sci. 216 (2003) 1–11.
[11] S. Eloot, D. De Wachter, I. Van Tricht, P. Verdonck, Computational flow modeling in hollow-fiber dialyzers, Artif. Organs 26 (2002) 590–599.
[12] S. Eloot, Y. D'Asseler, P. De Bondt, P. Verdonck, Combining SPECT medical imaging and computational fluid dynamics for analyzing blood and dialysate flow in hemodialyzers, Int. J. Artif. Organs 28 (2005) 739–749.
[13] S. Eloot, J. Vierendeels, P. Verdonck, Optimisation of solute transport in dialysers using athree-dimensional finite volume model, Comp. Methods Biomech. Biomed. Eng. 9 (2006) 363–370.
[14] W. Ding, W. Li, S. Sun, X. Zhou, P.A. Hardy, S. Ahmad, D. Gao, Three-dimensional simulation of mass transfer in artificial kidneys, Artif. Organs 39 (2015) E79–E89.
[15] W. Ding, L. He, G. Zhao, H. Zhang, Z. Shu, D. Gao, Double porous media model for mass transfer of hemodialyzers, Intern, J. Heat Mass Transf. 47 (2004) 4849–4855.
[16] S. Eloot, P. Verdonck, Modeling of transport phenomena in an artificial kidney, in: M. Akay (Ed.), Wiley Encyclopedia of Biomedical Engineering, 2006, pp.1–24.
[17] D. Quemada, General features of blood circulation in narrow vessels, in: C.M. Rokkiewcz (Ed.), Arteries and Arterial Blood Flow: Biological and Physiological Aspects, Springer-Verlag, Wien, 1983.
[18] R.B. Bird, W.E. Stewart, E.N. Lightfoot, Transport Phenomena, J. Wiley & Sons, Inc.,

New York, 2002.
[19] N.C. Brinkman, A calculation of the viscous force exerted by a flowing fluid on a dense swarm of particles, Appl. Sci. Res. A 1 (1947) 27–34.
[20] A.L. Zydney, Bulk mass transport limitations during high flux hemodialysis, Artif. Org. 17 (1993) 919–924.
[21] E.M. Landis, J.R. Pappenheimer, Handbook of Physiology, Section 2: Circulation, Am. Phys. Soc., Washington, DC, 1963.
[22] R.L. Fournier, Basic Transport Phenomena in Biomedical Engineering, 3rd ed., CRC Press, Boca Raton, 2012.
[23] A. Apelblat, A. Katzir-Katchalsky, A. Silberberg, A mathematical analysis of capillary tissue fluid exchange, Biorheology 11 (1974) 1–49.
[24] A.H. Kirsch, R. Lyko, L. Nilsson, W. Beck, M. Amdahl, P. Lechner, A. Schneider, C. Wanner, A.R. Rosenkranz, D.H. Krieter, Performance of hemodialysis with novel medium cut-off dialyzers, Nephrol. Dial. Transplant. 0 (2016) 1–8.
[25] A.T. Azar, Increasing dialysate flow rate increases dialyzer urea clearance and dialysis efficiency: an in vivo study, Saudi J. Kidney Dis. Transpl. 20 (2009) 1023–1029.
[26] R. Ouseph, C.A. Hutchison, R.A. Ward, Differences in solute removal by two high-flux membranes of nominally similar synthetic polymers, Nephrol. Dial. Transplant. 23 (2008) 1704–1712.
[27] R.J. Whittaker, R. Booth, R. Dyson, C. Bailey, L.P. Chini, S. Naire, S. Payvandi, Z. Rong, H. Woolard, L.J. Cummings, S.L. Waters, L. Mawasse, J.B. Chauduri, M.J. Ellis, V. Michael, N.J. Kuiper, S. Cartmell, Mathematical modelling of fibre-enhanced perfusion inside a tissue-engineering bioreactor, J. Theor. Biol. 256 (2009) 533–546.
[28] J.K. Leypoldt, Solute fluxes in different treatment modalities, Nephrol. Dial. Transplant. 15 (2000) 3–9.
[29] A. Granger, G. Vantard, J. Vantelon, B. Perrone, A mathematical approach of simultaneous dialysis and filtration (SDF), Proc. Eur. Soc. Artif. Organs 5 (1978) (174-17).
[30] J.P. Bhimani, R. Ouseph, R.A. Ward, Effect of increasing dialysate flow rate on diffusive mass transfer of urea, phosphate and β2-microglobulin during clinical haemodialysis, Nephrol. Dial. Transplant. (2010) 1–6.
[31] A.C. Yamashita, R. Fujita, N. Tomisawa, Y. Jinbo, M. Yamamura, Effect of packing density of hollow fibers on solute removal performances of dialyzers, Hemodial. Intern. 13 (2009) S2–S7.
[32] R.A. Ward, R. Ouseph, Modification of membrane characteristics allows a reduction in dialyzer membrane area without loss of performance, J. Am. Soc. Nephrol. 18 (2007).